Annals of Biomedical Engineering, Vol. 46, No. 12, December 2018 *(© 2018)* pp. 2023–2035
https://doi.org/10.1007/s10439-018-2101-z

Computational Fluid Dynamics Study of the Effects of Surface Roughness on Permeability and Fluid Flow-Induced Wall Shear Stress in Scaffolds

DAVAR ALI and SADRI SEN

Department of Mechanical Engineering, Faculty of Engineering, Ataturk University, Erzurum, Turkey

(Received 3 February 2018; accepted 17 July 2018; published online 20 July 2018)

Associate Editor Ender Finol oversaw the review of this article.

Abstract—In this work, we investigated surface roughness effects on bone scaffold permeability and fluid flow-induced wall shear stress (WSS) using computational fluid dynamics (CFD) analysis. Scaffolds are made of interconnected microchannels, whose fluid flow can be examined from the perspective of fluid flow dynamics. Given that the roughness of microchannel surfaces serves a non-negligible function in the fluid dynamics within the channels, it is believed that the wall roughness of scaffolds can play an important role in their permeability and WSS. Given the criticality of permeability and WSS in the effective biological functioning of scaffolds, we investigated manufacturing-induced surface roughness effects on the two aforementioned biocompatibility characteristics. To this end, three scaffolds with square pores of different sizes (300, 600, and 900 μm) and identical porosity (63%) were designed. Six roughness levels (0, 4, 8, 12, 16, and 20 μm) were established for the scaffold walls, thus enabling us to develop 18 scaffold models. The pressure drop and WSS in the scaffolds were then measured by CFD. Scaffold permeability was calculated using Darcy's law, with reference to geometrical parameters and the pressure drop derived from the CFD analysis. In all the scaffolds, high roughness decreased permeability and WSS. A significant difference in WSS reduction was found between the models with smooth scaffolds and the models with scaffolds that had a roughness of 20 μm. Except for the scaffold with a pore size of 300 μm, all the others showed no considerable change in permeability at different roughness levels.

Keywords—Scaffolds, Permeability, Wall shear stress, Surface roughness, CFD analysis.

INTRODUCTION

In recent years, the use of porous scaffolds in the regeneration and treatment of damaged organs has drawn considerable attention in the field of tissue engineering. Meanwhile, newly developed manufacturing technologies, such as additive manufacturing (AM), have enabled the production of three-dimensional scaffolds with a wide range of materials and different architectures that mimic host tissues.[2] Despite these valuable advancements, however, the characterization of the mechanical and biological properties of scaffolds remains a challenging task.

Evaluating biocompatibility characteristics, such as permeability[26] and WSS,[7] is critical because of their influence on cell bioactivity within scaffolds. A permeable scaffold should allow the sufficient diffusion of nutrients, gases and the adequate emission of waste through its pores.[36] Given that cell proliferation within scaffolds is directly influenced by permeability, its calculation is highly consequential in the optimization of cell culturing and the duration of treatment, regardless of the fact that permeability can exert contradictory effects on different types of cells.[22]

Cells with adequate signals, including biophysical stimuli, initiate the formation of desired tissue within a scaffold's pores.[20] Among well-known biological stimuli, the stress[42] and strain[27] that arise from fluid flow and mechanical loading on scaffolds, respectively, are the most noteworthy. Because WSS can exert different effects on diverse cells, examining its magnitude and modality in scaffold design is critical.[12,32,46] For example, researchers widely acknowledged that mechanical stimulation that includes shear stress can improve osteogenic differentiation.[9,46]

Many studies have been conducted to investigate the parameters that determine permeability and WSS.[7,11,16,24,25,35,37] Research has been devoted to determining the effects of scaffold structures on permeability on the basis of porosity pore size and pore shape.[8] In other fields, finite element analysis (FEA) has been evaluated as a powerful tool for characteriz-

Address correspondence to Davar Ali, Department of Mechanical Engineering, Faculty of Engineering, Ataturk University, Erzurum, Turkey. Electronic mail: daverali@atauni.edu.tr

0090-6964/18/1200-2023/0 © 2018 Biomedical Engineering Society

ing materials[3,4]; as a variant of FEA, computational fluid dynamics (CFD) is an effective alternative to complicated and expensive experimental tests in investigations of fluid behavior.[17] In numerical analysis techniques, such as FEA and CFD, computer-aided design (CAD) models are commonly used, but the manufacturing-induced differences between these models and actual scaffolds are often ignored. A few studies have generated realistic results on fluid flow within scaffolds with the use of CAD models. Dias *et al*., for example, found that experiments generate permeability values that are lower than those produced in CFD modeling.[15] Using CFD analysis, Truscello *et al*. explained the major mismatch in permeability results between CAD-based and micro-CT scanned (models made of high-resolution micro-CT images of manufactured scaffolds) models. The authors identified the interior surface roughness of the micro-CT models as one of the possible causes of the discrepancy between the models.[40] Although these studies provided useful insights, to the best of our knowledge, no research has been directed toward examining the effects of scaffold surface roughness on scaffold permeability and WSS. Due to the direct effect of permeability and WSS in the scaffolds on cellular activity within them,[11,41] the prediction of the exact magnitudes of these parameters in CFD analysis using similar geometries of the manufactured scaffolds can act as a step forward in their design.

Scaffolds are made of interconnected microchannels, whose underlying fluid flow dynamics can be used as basis in evaluating scaffold permeability. Given that fluid flow within a microchannel depends on the microchannel's dimensions, geometry, and other factors, such as wall roughness.[38] For example, Guo *et al*. found that the friction factor increased to about 11.4% in a microchannel (rectangular cross-section with dimensions of 500 × 500 μm) with a relative surface roughness of 4% under laminar flow.[19] Therefore, we can conclude that the permeability and WSS in scaffolds are not only controlled by pore architecture but also depend on other parameters, such as surface quality. On the basis of the assumption that the surface roughness of scaffolds plays a critical role in permeability and WSS, the current study carried out a CFD analysis of scaffolds with rough surfaces.

In representing the wall roughness of microchannels by CFD, simple elements are generally placed in the path of fluid flow; these barrier elements include rectangular, trapezoidal,[33] conical and sinusoidal[49] structures. Although models designed to predict the behavior of fluids in microchannels come with acceptable errors, the peaks and valleys of the surface topology that characterizes materials are naturally distributed in a random manner. Therefore, the CFD modeling of microchannel wall roughness with random topology can produce more accurate results. To generate surfaces with random topology, researchers developed fractal and Gaussian distribution[30] models.

In the present study, the surface roughness of scaffold microchannels were generated in ANSYS Parametric Design Language (APDL), and peak height and valley depth were generated using random Gaussian distribution. Scaffold models having square pores of different sizes (300, 600, and 900 μm) and identical porosity (63%) were prepared.[10] Six levels of roughness (R_a; 0, 4, 8, 12, 16, and 20 μm) were established for the scaffold walls; these roughness values were determined on the basis of the AM method, which is widely used in scaffold production.[44] To calculate the pressure drop and WSS in the scaffolds, CFD analysis was carried out in the laminar regime.

MATERIALS AND METHODS

Scaffold Models

The scaffold models were designed using SolidWorks. Figure 1a shows the 5 × 5×5 unit cells of the scaffolds and other relevant dimensions. As previously indicated, the R_a of the scaffolds ranged from 0 to 20 μm—a range that was based on the actual surface roughness values measured by conventional manufacturing methods (selective laser melting) for metallic scaffolds.[44] The generated rough surfaces R_a heights values were scattered highs scattered considering the Gaussian (normal) random distribution with mean value of 0 and a standard deviation of 0.333333. More details on generating a randomly rough surface can be found elsewhere.[39] Regarding the length and width of the scaffold walls, rough surfaces were generated using APDL. The generated rough surfaces and scaffolds were assembled to obtain the fluid domains (Fig. 1b). The models were assigned labels as P-(300-600-900)-(0-4-8-12-16-20) that are based on pore size and R_a. The P-300-16 model, for example, represents a scaffold with a pore size of 300 μm and a surface roughness of 16 μm.

The fluid domains that are instrumental to the examination of the effects exerted by surface roughness on scaffold permeability and WSS were generated. Owing to the symmetrical geometry of the unit cells and the need to avoid large-scale and expensive CFD analysis, only a quarter of the unit cells were used.

The solid and fluid domains and the boundary conditions of the scaffolds are shown in Fig. 2.

A symmetric boundary condition was assigned to the surfaces of neighbor scaffolds and the cutoffs in a quarter (Fig. 2).

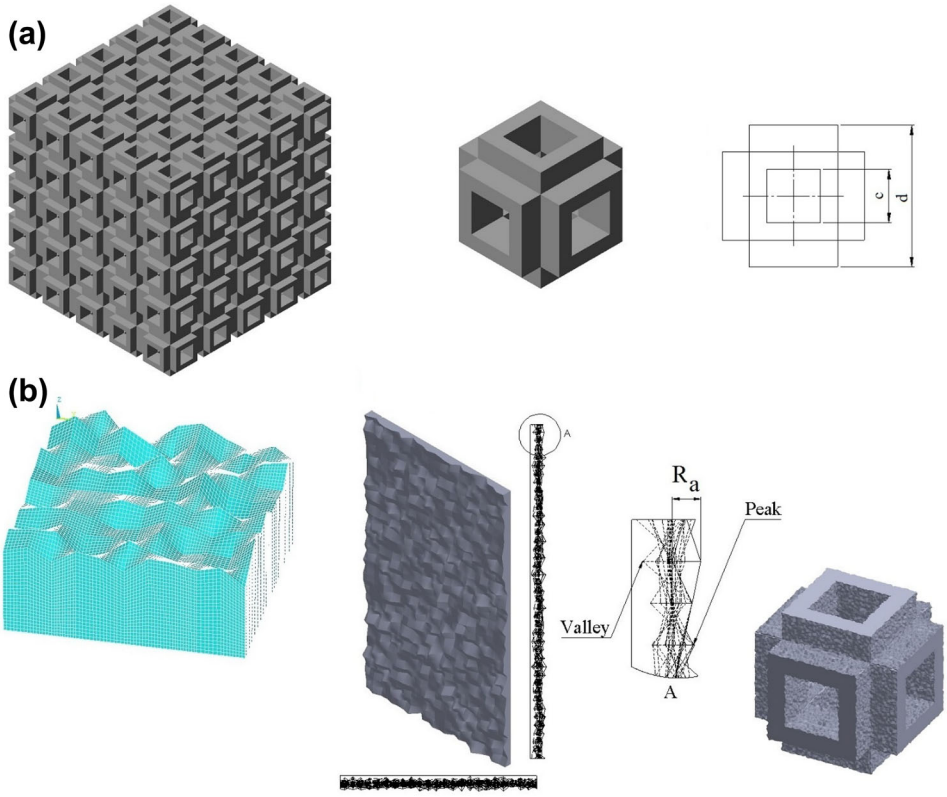

FIGURE 1. (a) The scaffold with 5 × 5×5 unit cells. For scaffolds P-300, P-600, and P-900, the d unit cell lengths were 800, 1600, and 2400 μm, and the c pore sizes were 300, 600, and 900 μm, respectively. (b) Rough surfaces were formed from randomly scattered peaks and valleys. Rough surfaces were produced in APDL by using the Gaussian distribution of R_a peaks. Rough walls were established for the scaffolds.

Governing Equations in CFD Analysis

Water was selected as the working fluid, after which a flow velocity of 0.001 m/s[25] was assigned to the inlet. The Reynolds number was calculated as follows:

$$\mathrm{Re} = \frac{\rho v D_{\mathrm{Pores}}}{\mu}, \tag{1}$$

where ρ, v, D_{Pores}, and μ represent the density of fluids (1000 kg/m^3), the inlet velocity (0.001 m/s), the hydraulic diameter (m) of pores, and the dynamic viscosity of water (0.001 Pa.s), respectively. For three groups of models, the Re was < 10, thus confirming the validity of Darcy's law.[40]

The Navier–Stokes equation for incompressible fluid dynamics[43] was used as a governing equation in the CFD analysis. The equation is expressed as follows:

$$\rho \frac{\partial u}{\partial t} - \mu \nabla^2 u + \rho(u.\nabla)u + \nabla p = F, \ \nabla.u = 0, \tag{2}$$

where u, ∇, and F denote the, the velocity of fluid flow (m/s), the del operator, and other forces (gravitational or centrifugal force), respectively.

Permeability (k) was calculated on the basis of Darcy's law[40] as follows:

$$k = \frac{Q\mu L}{A\Delta P} a \tag{3}$$

where Q, L, A, and ΔP represent the fluid flow rate (m^3/s), the model length (m), the cross-sectional area of a unit cell (m^2), and the pressure drop (Pa), respectively. It should be noted that the fluid viscosity in the scaffolds can be influenced by different factors such as polarization and electrically charged pores' walls [1]; however, to simplify this study, the viscosity was considered constant.[40]

Solution and Convergence

Using ANSYS Fluent, laminar analysis was performed to measure the pressure drop and fluid flow-induced WSS within the scaffolds. Tetrahedral elements were used to mesh the models.[17] To mesh rough surfaces, the rest of the models' maximum element sizes (i.e., 2 and 40 μm) were used. To determine the sensitivity of the CFD results to mesh quality, con-

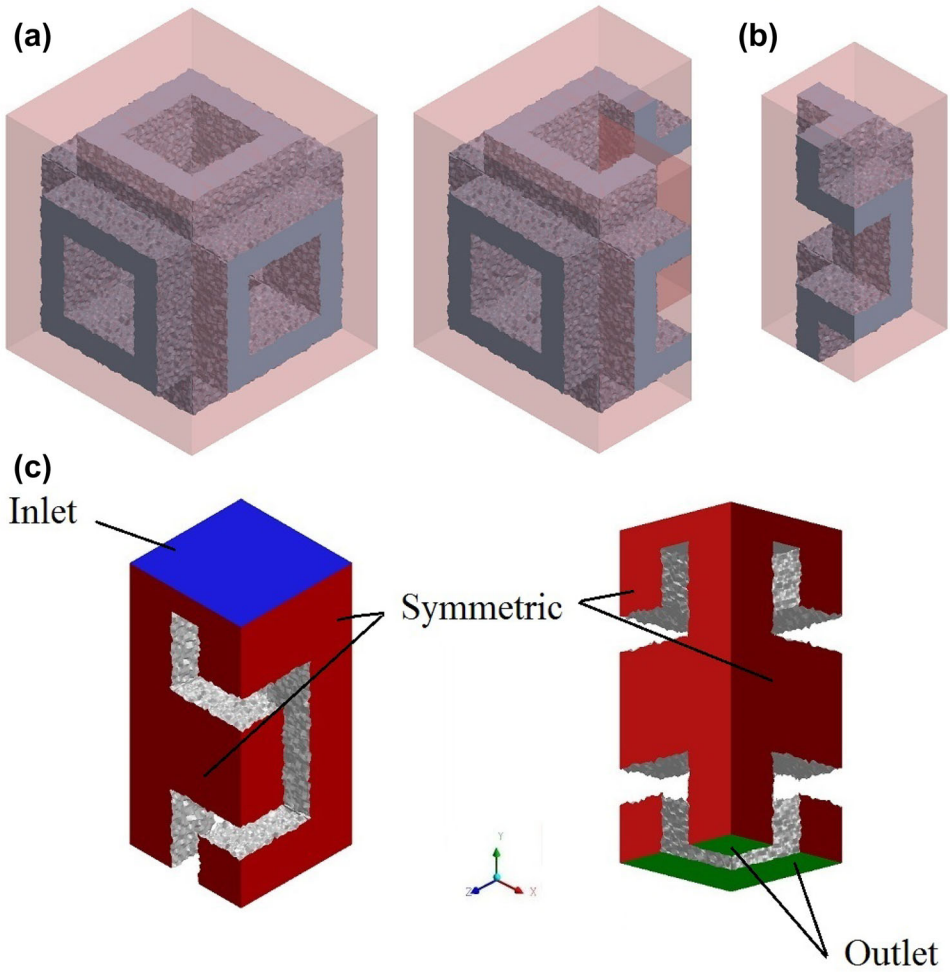

FIGURE 2. (a) Solid (grey) and fluid (pink) domains; (b) a quarter of the solid and fluid domains; (c) the fluid domain that was used in the CFD analysis; the top face (blue), side faces (red), bottom faces (green), and interior rough surface (gray) boundaries were denoted as the inlet, symmetry, outlet, and no-slip walls, respectively.

vergence analysis was performed for each model using residual criterion value of 1e-6.

The elements in the models are presented in Table 1.

As illustrated in Fig. 3, very fine mesh sizes were selected to obtain accurate feedback regarding the effects of wall roughness topology.

A metallic-based assumption of scaffolds that had a negligible deformation[47,48] during fluid flow allowed us to ignore a possible fluid–wall interaction in the CFD analysis.

RESULTS

Validation

To confirm the reliability of the determined surface roughness effects on pressure drop, a similar model examined by Guo *et al.*[19] was redesigned with a rough surface. Very good agreement was observed between the results, with an error of 1.61% in the Poiseuille number (Table 2).

Permeability and WSS

To illuminate the modality of pressure distribution, contours were ascertained for the 300-0 and 300-20 models (Fig. 4). Figure 4b indicates that the presence of rough surfaces in the 300-20 model caused a pressure drop that was higher than that occurring in the smooth walls of the 300-0 model. To probe into the reliability and performance of the models in the CFD analysis, their pressure drop (ΔP) responses to flow rate were tested under four different inlet velocities (5, 10, 15, and 20 mm/s). Figure 4c shows the linear curve-fitting graph of the assigned inlet velocity and the ΔP measured for the smooth models and the models with a 20 μm surface roughness. In all the

TABLE 1. Number of elements for the CFD analysis.

	P-300						P-600					
Pore size												
R_a	0	4	8	12	16	20	0	4	8	12	16	20
Number of elements	1119129	1320756	1977322	2316358	2964502	3493566	2191063	2534679	2898957	3898389	4992108	5155438

	P-900				
Pore size					
R_a	0	4	8	12	16	20
Number of elements	3448505	3605706	3823073	4794738	6978981	7262839

models, pressure drop correlated well with inlet velocity ($R^2 > 0.99$).

With reference to Eq. (3) and the obtained ΔP between the inlet and outlet in the CFD models, the permeability of each scaffold was calculated (Fig. 5).

Regardless of the effects of surface roughness on scaffold permeability, such permeability increased with increasing pore size (Fig. 5) a trend that is consistent with the literature.[5,7] Because this study was aimed primarily at examining the effects exerted by the surface quality of scaffold walls on permeability and WSS, the effects of pore size were minimally explored.

The intergroup assessment of the scaffolds indicated that the maximum difference in permeability occurred in the P-300 group, specifically between the P-300-0 and P-300-20 models, with a 22.19% decrease in permeability. Minimal changes occurred in the P-600 and P-900 groups, with slight differences of 3.55 and 2.3% between the models with R_a values of 0 and 20 μm. As reflected in Eq. (3), the decrease in permeability was the result of the pressure drop (ΔP) increase that arose from surface roughness. In all the three groups of scaffolds, however, a surface roughness of up to 12 μm did not exert any significant effects on permeability. Although no definitive method has been developed to calculate the effects of surface roughness on pressure drop for microchannels, many studies have shown that a pressure drop can be observed when relative surface roughness (the ratio of surface roughness to hydraulic diameter) passes a certain threshold.[13,14,19] In the current research, for example, the relative surface roughness levels of models P-300-12, P-600-12, and P-900-12 were are 4, 2, and 1.33%, respectively. Note that in this work, the Reynolds number was very low, and the scaffolds were composed of tortuous microchannels. Therefore, the permeability results for the scaffolds with small relative surface roughness levels are expected and aligned with the findings of similar studies on microchannels.[14]

As stated previously, WSS plays a major role in stimulating cell proliferation within scaffolds. Thus, the WSS of the models was determined on the basis of an inlet velocity of 1 mm/s. The changes in WSS in all the models are illustrated in Fig. 6.

The average magnitude of WSS decreased with increasing pore size a tendency that aligns with similar analysis results derived by Zhao *et al.*[50] With respect to the effects of surface roughness on WSS, increasing roughness decreased WSS; the maximum difference in WSS occurred between P-900-0 and P-900-20, with a reduction of 26.92%. The P-600-20to P-600-0 models and the P-300-20 to P-300-0 models registered a 25.49 and 17.94% decrease in WSS, respectively. The average WSS values are useful, but a more comprehensive understanding of the effects of roughness on WSS

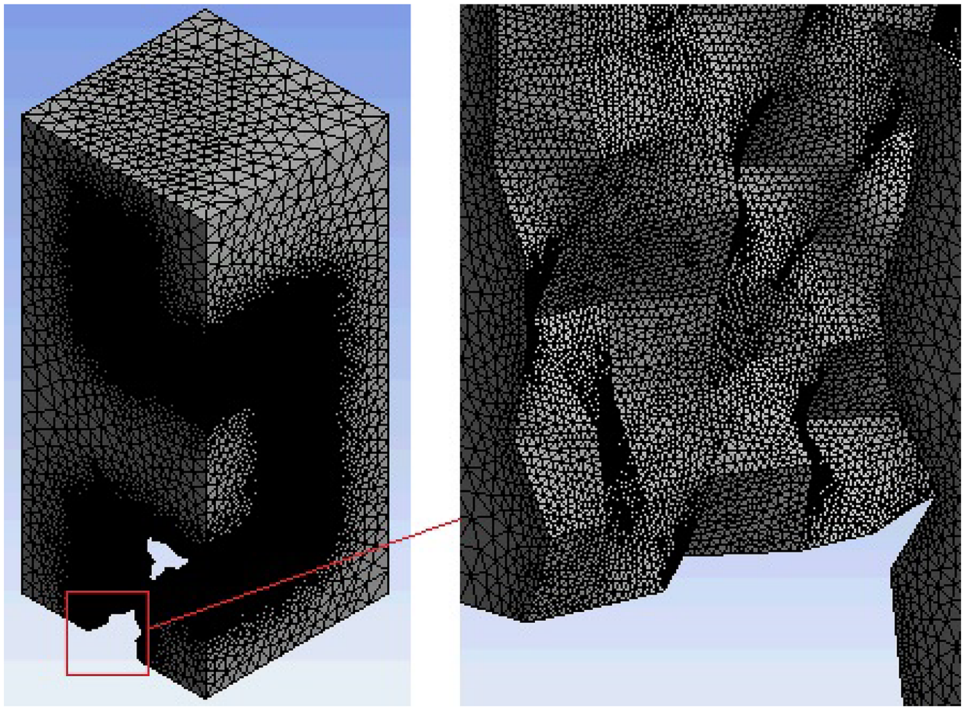

FIGURE 3. The P-300-20 model and refined mesh in the wall surfaces.

TABLE 2. Poiseuille numbers for our model and Guo *et al.*'s work with a Reynolds number of 100.

Model	Cross-section	Length (mm)	R_a (μm)	Poiseuille number	Error (%)
Guo *et al.* work	500 × 500 μm	20	24	62	1.61
Current study	500 × 500 μm	20	24	61	

necessitates its scattering on models walls area with zero and 20 μm of roughness was showed in Fig. 7.

All the six models exhibited the same pattern in their WSS distribution histograms (Fig. 7)—a finding that corresponds with the results in the literature.[23] A right-skewed histogram indicates that a huge percentage of a scaffold's wall is exposed to a WSS that is lower than mean values. The tendency to skew to the right was more pronounced in the scaffolds with a 20 μm roughness than in the scaffolds with zero roughness. This result reflects that more surfaces were exposed to a WSS lower than the mean value in the rough models than in the smooth scaffolds.

DISCUSSION

It is generally accepted that among the effective parameters on the permeability of the scaffolds, porosity plays the most important role. However, in this study to focus only on surface roughness effects on permeability and WSS of the scaffolds, the porosity of all models was constant and the size of the pores varied..[1] Rather than being influenced by surface roughness, scaffold permeability and WSS are strongly affected by pore size. However, because researchers have reached no agreement with respect to ideal pore size (reported sizes vary between 200 and 1300 μm[31] in the literature), all factors that can potentially affect the successful design and implementation of scaffolds, including permeability and WSS, should be investigated under different pore sizes. An explanation of the relationship between surface roughness and permeability or WSS appears to provide additional insight into scaffold design and characterization.

Theoretically, friction in a wall and, consequently, the changes in pressure drop in microchannels can be described on the basis of the (i) increase in shear stress and (ii) the obstruction of sections.[21] The physical presence of rough elements on walls causes partial obstruction in cross-sections and deflects fluid flow from its normal path in the vicinity of walls (Fig. 8). Considering these issues, results in a straightforward interpretation of pressure drop results.

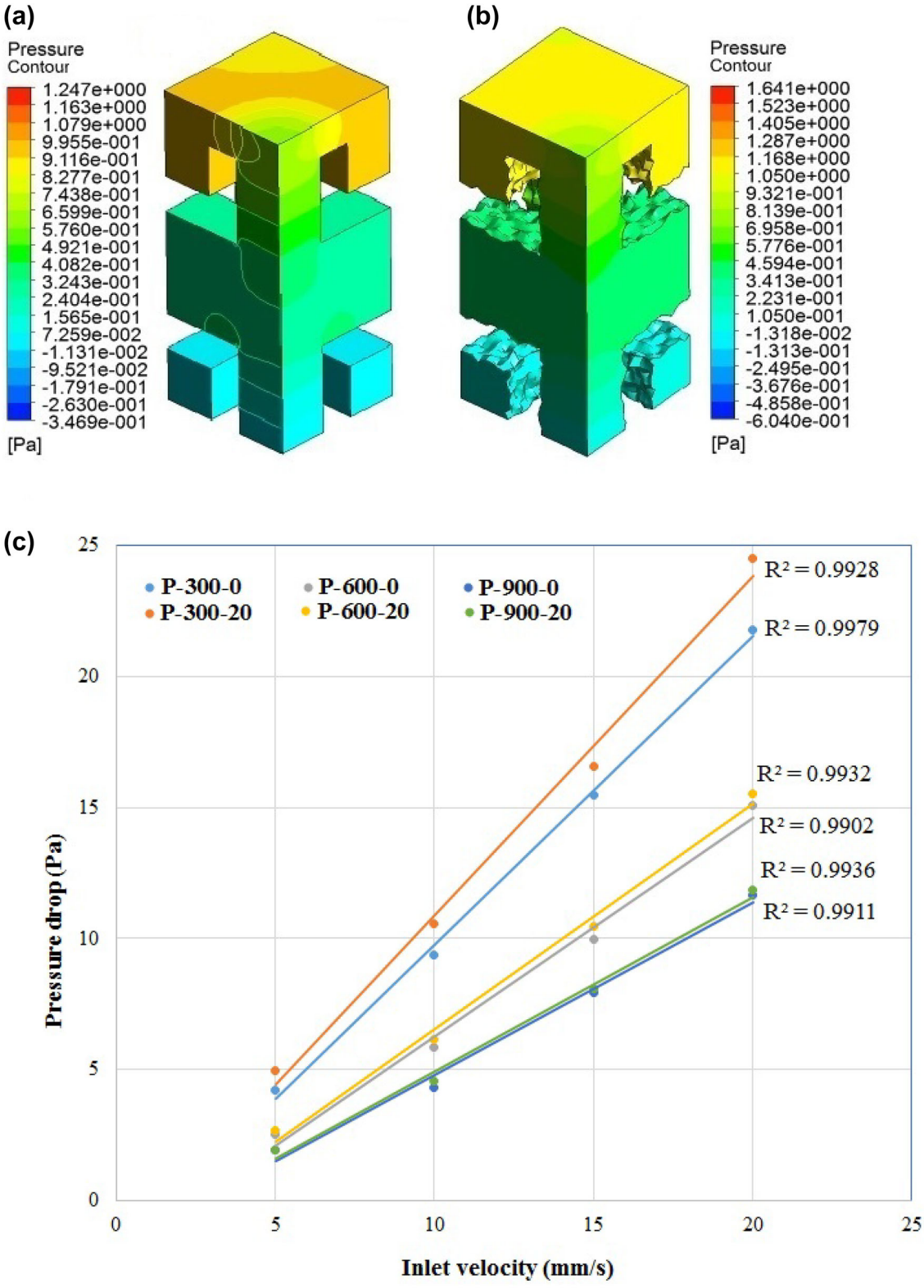

FIGURE 4. Pressure contours at an inlet velocity of 1 mm/s; (a) pressure contour of 300-0 and (b) pressure contour of 300-20; (c) correlation between pressure drop and inlet velocity the P-300-0, P-300-20, P-600-0, P-600-20, P-900-0 and P-900-20 scaffolds.

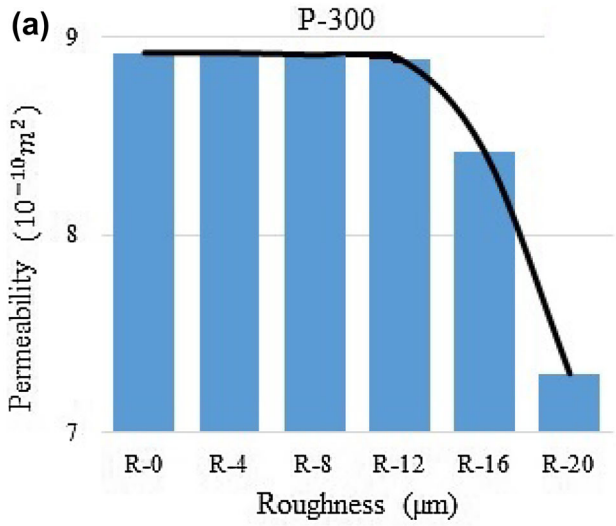

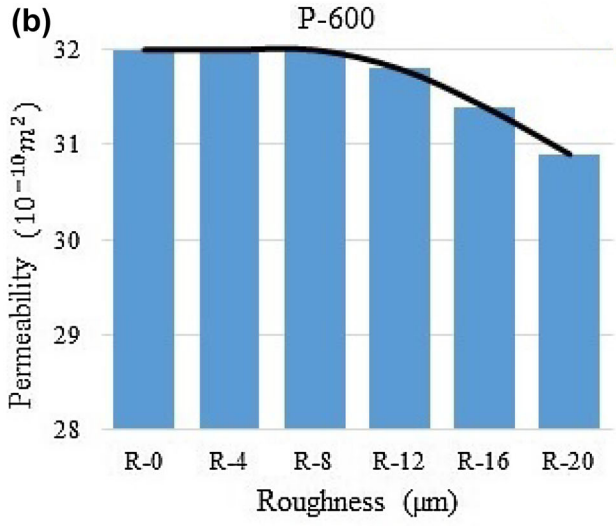

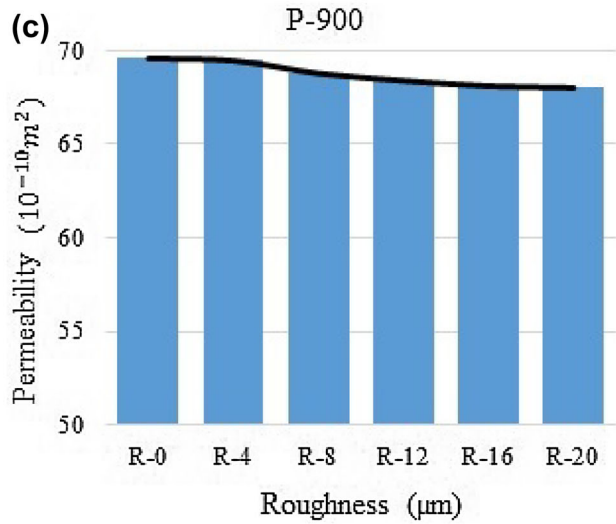

FIGURE 5. Permeability changes vs. roughness in the (a) P-300, (b) P-600 and (c) P-900 scaffolds.

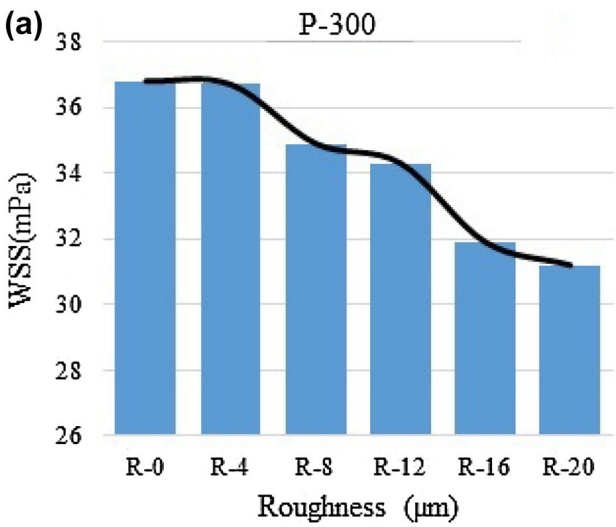

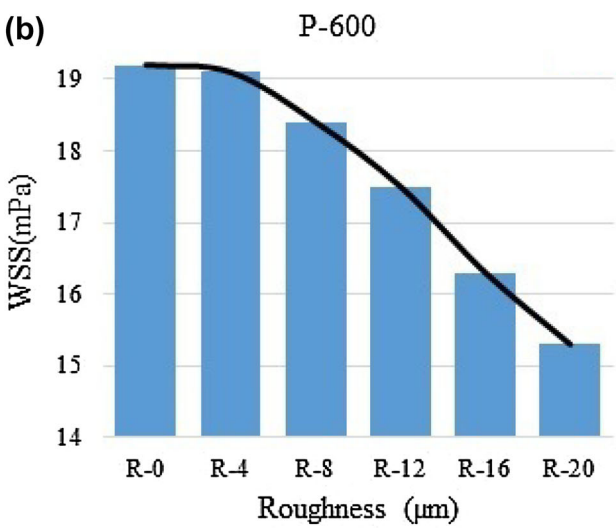

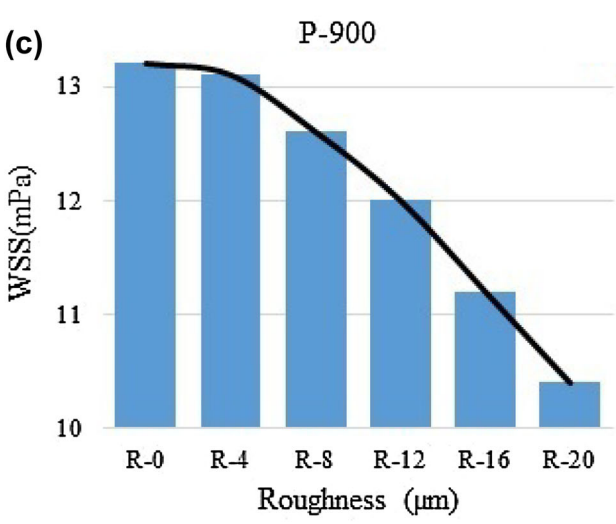

FIGURE 6. WSS changes vs. roughness in the (a) P-300, (b) P-600 and (c) P-900 scaffolds. The graph shows only the average WSS values.

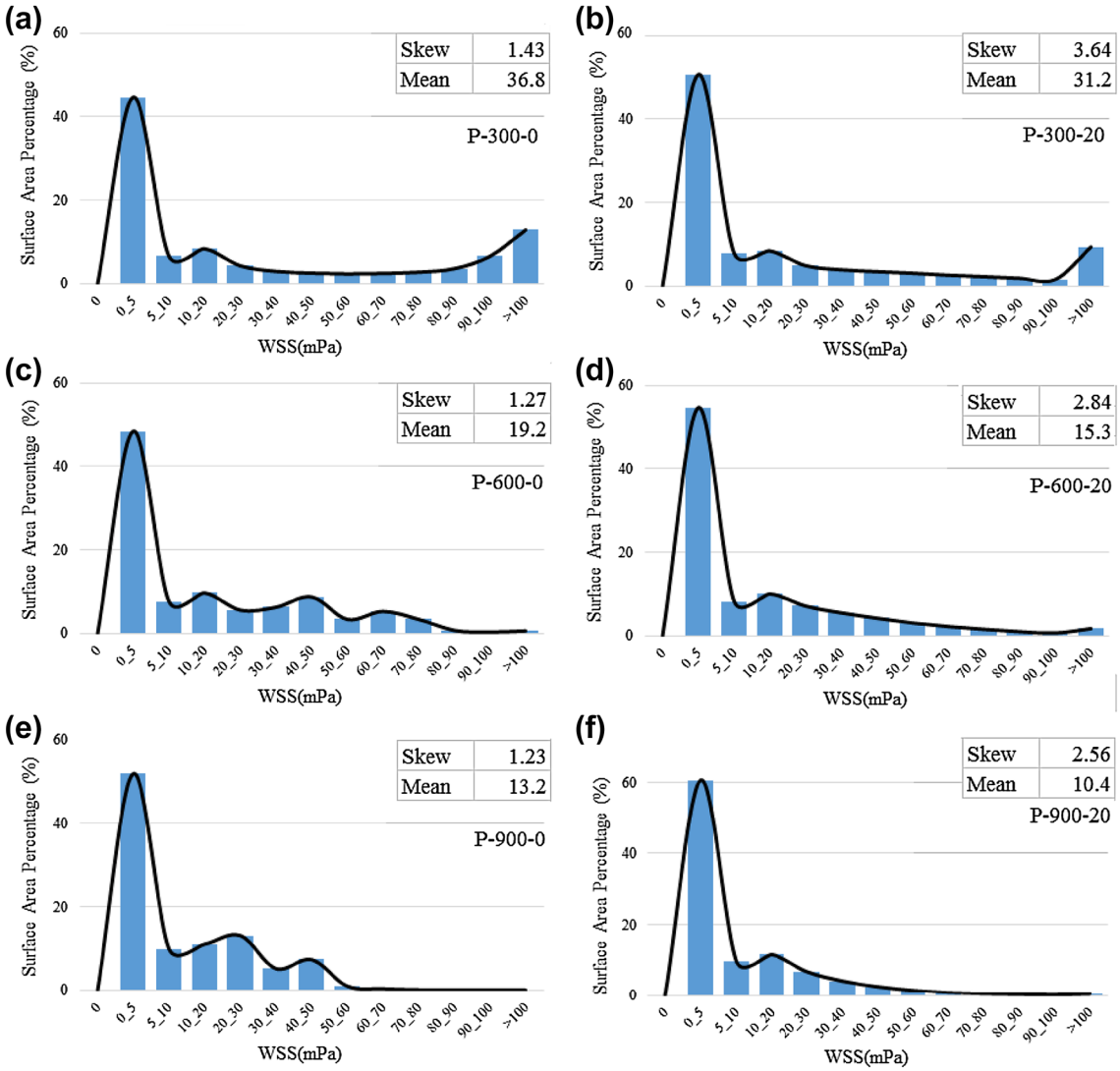

FIGURE 7. WSS distributions in the (a) P-300-0, (b) P-300-20, (c) P-600-0, (d) P-600-20, (e) P-900-0, and (f) P-900-20 scaffolds. The distributions were induced by a velocity of 1 mm/s.

A layer of fluid with a velocity close to 0 was observed in both models. Owing to the presence of corrugated rough elements in P-900-20 the thickness of this layer was slightly more prominent.

Many theoretical[30,38] and experimental[45] works have been reported in the literature, with studies considering hydraulic diameter as the most important factor in pressure drop. Accordingly, the results of the current research can reasonably be evaluated in the same way. For example, the P-300-20 model exhibited a pressure drop greater than that occurring in the P-300-0 model (Fig. 4). This result is attributed to the lower hydraulic diameter caused by the presence of 20 μm roughness elements throughout the scaffold's channels. The WSS reduction in the intergroup models can also be justified with the same standpoint. An increase in pressure drop in rough models indicates that a small section for fluid transfer throughout scaffolds exists within the models; the existence of this section reduces fluid flow rate in rough models (Table 3). On the other hand, WSS and fluid flow rate have a linear relationship[23]; thus, any reduction in velocity leads to a smaller WSS.

Contradictory fluid flows in the vicinity of peaks and valleys were also observed in the rough models (Fig. 8c). This phenomenon may be due to the local microscopic vortices that were created when fluid collided with the peaks.[19] Understanding the biological effects of this interesting phenomenon on cell culturing necessitates further studies.

With respect to cell activity within the scaffolds, the effects of rough surfaces can be evaluated from two

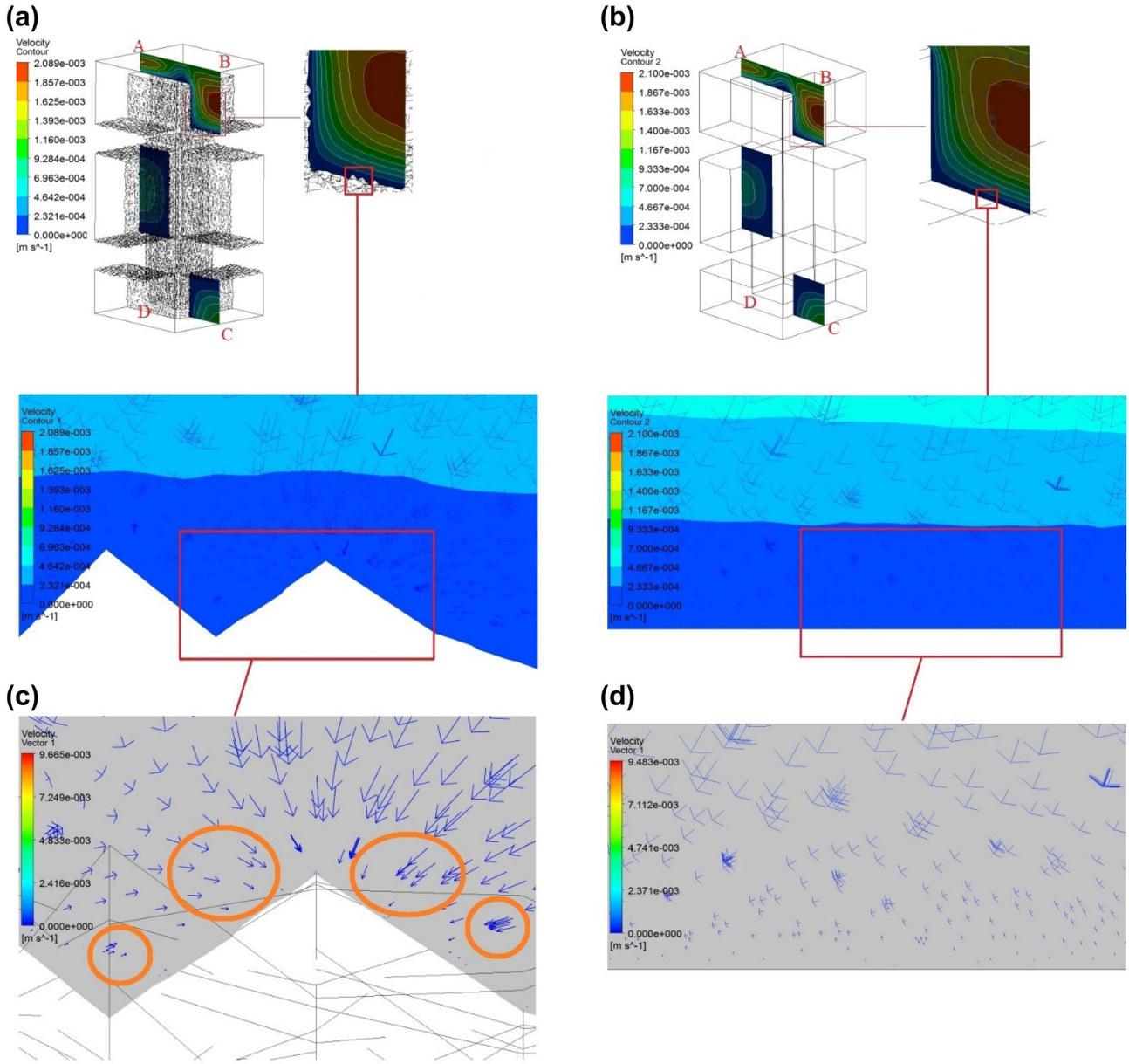

FIGURE 8. Velocity contours in the (a) P-900-20 and (b) P-900-0 models under an inlet velocity of 1 mm/s in the ABCD plane. (c) Contradictory fluid flows on both sides of a peak (marked with orange ellipsoids). (d) Regular fluid flow in the vicinity of a smooth wall.

TABLE 3. Differences in outlet velocities between rough and smooth scaffolds.

Models	Inlet velocity (mm/s)	Outlet velocity (mm/s)	Decrease (%)
P-300-0	1.00	0.505	49.5
P-300-20		0.386	61.4
P-600-0		0.500	50
P-600-20		0.409	59.1
P-900-0		0.490	51
P-900-20		0.423	57.7

contradictory points of view: (i) For the primary attachment of cells, rough surfaces potentially create favorable sites because they possess a higher number of corners.[34] (ii) Reducing permeability can slow down cell growth.[41] The present study suggests that for scaffolds with small pores, surface roughness can be an inhibiting factor that causes channel occlusion, which in turn, inhibits cell growth. Some issues worth noting are that only the partial occlusion of scaffold pores can be related to their surface roughness and that their complete obstruction during cell culturing depends on cell differentiation and proliferation.[6,18] For scaffolds with large pores, however, surface roughness serves not only as a deterrent but also, under the presence of numerous corners, as a driver of initial cell attachment. Nevertheless, the chemistry (hydrophobic or hydrophilic), along with the topology, of a scaffold surface can play the primary role in the initial absorption of proteins (Vroman effect) on the scaffold walls.[28,29]

CONCLUSION

On the basis of fluid flow dynamics, the effects of surface roughness on the permeability and WSS of scaffolds were investigated. The results of this study introduced surface roughness as a new parameter that can potentially affect the fluid flow dynamics within porous scaffolds in tissue engineering. The results are summarized as follows:

(i) Although the effects of pore size on permeability were far more substantial than the surface roughness effects, the latter's influence on the scaffolds with small pore sizes was non-negligible.
(ii) The effects of surface roughness on the permeability of the models with 300 μm pores were more significant than those on the scaffolds with larger pore sizes. Nevertheless, the effects of surface roughness on the WSS of the models with 600 and 900 μm pores were more pronounced than those on the WSS of the model with 300 μm pores.
(iii) The contradictory fluid flow in the vicinity of the rough walls requires more theoretical and experimental studies to illuminate its effects on cell culturing.
(iv) We endeavored to demonstrate the effects of surface roughness on a common architecture of the scaffolds. However, clarifying the effects of surface roughness on permeability and WSS necessitates more studies, especially those that consider different scaffold architectures.

ACKNOWLEDGMENTS

This research has been supported by Ataturk University. The authors would like to thank the Ataturk University for funding and Dr. Kamil Kabakus for technical assistance.

CONFLICT OF INTEREST

The authors declare no conflicts of interest.

REFERENCES

[1]Abdalrahman, T., S. Scheiner, and C. Hellmich. Is trabecular bone permeability governed by molecular ordering-induced fluid viscosity gain? Arguments from re-evaluation of experimental data in the framework of homogenization theory. *J. Theor. Biol.* 365:433–444, 2015.
[2]Ahmadi, S. M., S. A. Yavari, R. Wauthle, B. Pouran, J. Schrooten, H. Weinans, and A. A. Zadpoor. Additively manufactured open-cell porous biomaterials made from six different space-filling unit cells: the mechanical and morphological properties. *Materials* 8:1871–1896, 2015.
[3]Ali, D., and S. Sen. Finite element analysis of the effect of boron nitride nanotubes in beta tricalcium phosphate and hydroxyapatite elastic modulus using the RVE model. *Compos. Part B* 90:336–340, 2016.
[4]Ali, D., and S. Sen. Finite element analysis of boron nitride nanotubes' shielding effect on the stress intensity factor of semielliptical surface crack in a wide range of matrixes using RVE model. *Compos. Part B* 110:351–360, 2017.
[5]Ali, D., and S. Sen. Finite element analysis of mechanical behavior, permeability and fluid induced wall shear stress of high porosity scaffolds with gyroid and lattice-based architectures. *J. Mech. Behav. Biomed. Mater.* 75:262–270, 2017.
[6]Ayati, B. P., C. M. Edwards, G. F. Webb, and J. P. Wikswo. A mathematical model of bone remodeling dynamics for normal bone cell populations and myeloma bone disease. *Biol. Direct* 5:28, 2010.
[7]Bartnikowski, M., T. J. Klein, F. P. W. Melchels, and M. A. Woodruff. Effects of scaffold architecture on mechanical characteristics and osteoblast response to static and perfusion bioreactor cultures. *Biotechnol. Bioeng.* 111:1440–1451, 2014.
[8]Blanquer, S. B. G., M. Werner, M. Hannula, S. Sharifi, G. P. R. Lajoinie, D. Eglin, J. Hyttinen, A. A. Poot, and D. W. Grijpma. Surface curvature in triply-periodic minimal surface architectures as a distinct design parameter in preparing advanced tissue engineering scaffolds. *Biofabrication* 9:025001, 2017.
[9]Brindley, D., K. Moorthy, J.-H. Lee, C. Mason, H.-W. Kim, and I. Wall. Bioprocess forces and their impact on cell behavior: implications for bone regeneration therapy. *J. Tissue Eng.* 2011:620247, 2011.
[10]Cavo, M., and S. Scaglione. Scaffold microstructure effects on functional and mechanical performance: integration of theoretical and experimental approaches for bone tissue engineering applications. *Mater. Sci. Eng. C* 68:872–879, 2016.

[11]Chen, G. B., R. Xu, C. Zhang, and Y. G. Lv. Responses of MSCs to 3D scaffold matrix mechanical properties under oscillatory perfusion culture. *ACS Appl. Mater. Interfaces.* 9:1207–1218, 2017.
[12]Conway, D. E., M. T. Breckenridge, E. Hinde, E. Gratton, C. S. Chen, and M. A. Schwartz. Fluid shear stress on endothelial cells modulates mechanical tension across VE-cadherin and PECAM-1. *Curr. Biol.* 23:1024–1030, 2013.
[13]Croce, G., and P. D'Agaro. Numerical simulation of roughness effect on microchannel heat transfer and pressure drop in laminar flow. *J. Phys. D* 38:1518–1530, 2005.
[14]Dai, B. M., M. X. Li, and Y. T. Ma. Effect of surface roughness on liquid friction and transition characteristics in micro- and mini-channels. *Appl. Therm. Eng.* 67:283–293, 2014.
[15]Dias, M. R., P. R. Fernandes, J. M. Guedes, and S. J. Hollister. Permeability analysis of scaffolds for bone tissue engineering. *J. Biomech.* 45:938–944, 2012.
[16]Egan, P. F., S. J. Ferguson, and K. Shea. Design of hierarchical three-dimensional printed scaffolds considering mechanical and biological factors for bone tissue engineering. *J. Mech. Des.* 139:061401, 2017.
[17]Gómez, S., M. D. Vlad, J. López, and E. Fernández. Design and properties of 3D scaffolds for bone tissue engineering. *Acta Biomater.* 42:341–350, 2016.
[18]Graham, J. M., B. P. Ayati, S. A. Holstein, and J. A. Martin. The role of osteocytes in targeted bone remodeling: a mathematical model. *PLoS ONE* 8:10, 2013.
[19]Guo, L., H. Xu, and L. Gong. Influence of wall roughness models on fluid flow and heat transfer in microchannels. *Appl. Therm. Eng.* 84:399–408, 2015.
[20]Hendrikson, W. J., A. J. Deegan, Y. Yang, C. A. van Blitterswijk, N. Verdonschot, L. Moroni, and J. Rouwkema. Influence of additive manufactured scaffold architecture on the distribution of surface strains and fluid flow shear stresses and expected osteochondral cell differentiation. *Front. Bioeng. Biotechnol.* 5:6, 2017.
[21]Kandlikar, S. G., D. Schmitt, A. L. Carrano, and J. B. Taylor. Characterization of surface roughness effects on pressure drop in single-phase flow in minichannels. *Physics of Fluids* 17:100606, 2005.
[22]Kemppainen, J. M., and S. J. Hollister. Differential effects of designed scaffold permeability on chondrogenesis by chondrocytes and bone marrow stromal cells. *Biomaterials* 31:279–287, 2010.
[23]Lesman, A., Y. Blinder, and S. Levenberg. Modeling of flow-induced shear stress applied on 3D cellular scaffolds: implications for vascular tissue engineering. *Biotechnol. Bioeng.* 105:645–654, 2010.
[24]Lipowiecki, M., M. Ryvolova, A. Tottosi, N. Kolmer, S. Naher, S. A. Brennan, M. Vazquez, and D. Brabazon. Permeability of rapid prototyped artificial bone scaffold structures. *J. Biomed. Mater. Res. Part A* 102:4127–4135, 2014.
[25]Marin, A. C., and D. Lacroix. The inter-sample structural variability of regular tissue-engineered scaffolds significantly affects the micromechanical local cell environment. *Interface Focus* 5:8, 2015.
[26]Mitsak, A. G., J. M. Kemppainen, M. T. Harris, and S. J. Hollister. Effect of polycaprolactone scaffold permeability on bone regeneration in vivo. *Tissue Eng. Part A* 17:1831–1839, 2011.
[27]Miyashita, S., N. E. M. B. Ahmed, M. Murakami, K. Iohara, T. Yamamoto, H. Horibe, K. Kurita, T. Takano-Yamamoto, and M. Nakashima. Mechanical forces induce odontoblastic differentiation of mesenchymal stem cells on three-dimensional biomimetic scaffolds. *J. Tissue Eng. Regen. Med.* 11:434–446, 2017.
[28]Palacio, M. L. B., and B. Bhushan. Bioadhesion: a review of concepts and applications. *Philos. Trans. R. Soc. A* 370:2321–2347, 2012.
[29]Palacio, M., S. Schricker, and B. Bhushan. Morphology and protein adsorption characteristics of block copolymer surfaces. *J. Microsc.* 240:239–248, 2010.
[30]Pelević, N., and T. H. van der Meer. Heat transfer and pressure drop in microchannels with random roughness. *Int. J. Therm. Sci.* 99:125–135, 2016.
[31]Rahbari, A., H. Montazerian, E. Davoodi, and S. Homayoonfar. Predicting permeability of regular tissue engineering scaffolds: scaling analysis of pore architecture, scaffold length, and fluid flow rate effects. *Comput. Methods Biomech. Biomed. Eng.* 20:231–241, 2017.
[32]Rajendran, P., T. Rengarajan, J. Thangavel, Y. Nishigaki, D. Sakthisekaran, G. Sethi, and I. Nishigaki. The vascular endothelium and human diseases. *Int. J. Biol. Sci.* 9:1057–1069, 2013.
[33]Rawool, A. S., S. K. Mitra, and S. G. Kandlikar. Numerical simulation of flow through microchannels with designed roughness. *Microfluid. Nanofluid.* 2:215–221, 2006.
[34]Rumpler, M., A. Woesz, J. W. C. Dunlop, J. T. van Dongen, and P. Fratzl. The effect of geometry on three-dimensional tissue growth. *J. R. Soc. Interface* 5:1173–1180, 2008.
[35]Santamaría, V. A. A., M. Malvè, A. Duizabo, A. M. Tobar, G. G. Ferrer, J. M. G. Aznar, M. Doblaré, and I. Ochoa. Computational methodology to determine fluid related parameters of non regular three-dimensional scaffolds. *Ann. Biomed. Eng.* 41:2367–2380, 2013.
[36]Serpooshan, V., M. Julien, O. Nguyen, H. Wang, A. Li, N. Muja, J. E. Henderson, and S. N. Nazhat. Reduced hydraulic permeability of three-dimensional collagen scaffolds attenuates gel contraction and promotes the growth and differentiation of mesenchymal stem cells. *Acta Biomater.* 6:3978–3987, 2010.
[37]Sonam, S., S. R. Sathe, E. K. F. Yim, M. P. Sheetz, and C. T. Lim. Cell contractility arising from topography and shear flow determines human mesenchymal stem cell fate. *Sci. Rep.* 6:20415, 2016.
[38]Taylor, J. B., A. L. Carrano, and S. G. Kandlikar. Characterization of the effect of surface roughness and texture on fluid flow—past, present, and future. *Int. J. Therm. Sci.* 45:962–968, 2006.
[39]Thompson, M. K. Methods for the Generation of Rough Surfaces in ANSYS. Cambridge: Mechanical Engineering Department, MIT, 2006.
[40]Truscello, S., G. Kerckhofs, S. Van Bael, G. Pyka, J. Schrooten, and H. Van Oosterwyck. Prediction of permeability of regular scaffolds for skeletal tissue engineering: a combined computational and experimental study. *Acta Biomater.* 8:1648–1658, 2012.
[41]Van Bael, S., Y. C. Chai, S. Truscello, M. Moesen, G. Kerckhofs, H. Van Oosterwyck, J. P. Kruth, and J. Schrooten. The effect of pore geometry on the in vitro biological behavior of human periosteum-derived cells seeded on selective laser-melted Ti6Al4V bone scaffolds. *Acta Biomater.* 8:2824–2834, 2012.
[42]Voronov, R., S. VanGordon, V. I. Sikavitsas, and D. V. Papavassiliou. Computational modeling of flow-induced

shear stresses within 3D salt-leached porous scaffolds imaged via micro-CT. *J. Biomech.* 43:1279–1286, 2010.
[43]Vossenberg, P., G. A. Higuera, G. van Straten, C. A. van Blitterswijk, and A. J. B. van Boxtel. Darcian permeability constant as indicator for shear stresses in regular scaffold systems for tissue engineering. *Biomech. Model. Mechanobiol.* 8:499, 2009.
[44]Wang, D., Y. Liu, Y. Q. Yang, and D. M. Xiao. Theoretical and experimental study on surface roughness of 316L stainless steel metal parts obtained through selective laser melting. *Rapid Prototyp. J.* 22:706–716, 2016.
[45]Wang, G. L., D. W. Yang, Y. Wang, D. Niu, X. L. Zhao, and G. F. Ding. Heat transfer and friction characteristics of the microfluidic heat sink with variously-shaped ribs for chip cooling. *Sensors* 15:9547–9562, 2015.
[46]Wittkowske, C., G. C. Reilly, D. Lacroix, and C. M. Perrault. In vitro bone cell models: impact of fluid shear stress on bone formation. *Front. Bioeng. Biotechnol.* 4:87, 2016.
[47]Ali, D., and S. Sen. Permeability and fluid flow-induced wall shear stress of bone tissue scaffolds: computational fluid dynamic analysis using Newtonian and non-Newtonian blood flow models. *Comput. Biol. Med.* 99:201–208, 2018.
[48]Yan, C., L. Hao, A. Hussein, and P. Young. Ti–6Al–4V triply periodic minimal surface structures for bone implants fabricated via selective laser melting. *J. Mech. Behav. Biomed. Mater.* 51:61–73, 2015.
[49]Yousaf, M., and S. Usman. Natural convection heat transfer in a square cavity with sinusoidal roughness elements. *Int. J. Heat Mass Transf.* 90:180–190, 2015.
[50]Zhao, F. H., T. J. Vaughan, and L. M. McNamara. Quantification of fluid shear stress in bone tissue engineering scaffolds with spherical and cubical pore architectures. *Biomech. Model. Mechanobiol.* 15:561–577, 2016.